1   **Shared vulnerability for connectome alterations across psychiatric and neurological**

2   **brain disorders**

3

4   **Authors**

5   Siemon C. de Lange[1], Lianne H. Scholtens[1], Leonard H. van den Berg[2], Marco P. Boks[3],

6   Marco Bozzali[4,5], Wiepke Cahn[3], Udo Dannlowski[6], Sarah Durston[3], Elbert Geuze[3,7], Neeltje

7   E.M. van Haren[8], Manon H.J. Hillegers[3,9], Kathrin Koch[10,11], María Ángeles Jurado[12,13,14],

8   Matteo Mancini[15], Idoia Marqués-Iturria[12], Susanne Meinert[6], Roel A. Ophoff[3,16], Tim J.

9   Reess[10,11], Jonathan Repple[6], René S. Kahn[3,17] and Martijn P. van den Heuvel[1,18,*]

10   for the Alzheimer's Disease Neuroimaging Initiative[19]

11

12   [19] Data used in preparation of this article were obtained from the Alzheimer's Disease

13   Neuroimaging Initiative (ADNI) database (adni.loni.usc.edu). As such, the investigators

14   within the ADNI contributed to the design and implementation of ADNI and/or provided data

15   but did not participate in analysis or writing of this report. A complete listing of ADNI

16   investigators can be found at: http://adni.loni.usc.edu/wp-

17   content/uploads/how_to_apply/ADNI_Acknowledgement_List.pdf

18

19   **Affiliations**

20   [1] Department of Complex Trait Genetics, Center for Neurogenomics and Cognitive Research,

21   Amsterdam Neuroscience, VU University Amsterdam, Amsterdam, The Netherlands

22   [2] Brain Center Rudolf Magnus, Department of Neurology, University Medical Center

23   Utrecht, Utrecht, The Netherlands

24   [3] Brain Center Rudolf Magnus, Department of Psychiatry, University Medical Center

25   Utrecht, Utrecht, The Netherlands

26   [4] Department of Neuroscience, Brighton and Sussex Medical School, University of Sussex,

27   Brighton, East Sussex, UK

28   [5] Neuroimaging Laboratory, Santa Lucia Foundation IRCCS, Rome, Italy

29   [6] Department of Psychiatry, University of Muenster, Muenster, Germany

30   [7] Research Center Military Mental Healthcare, Utrecht, The Netherlands

31   [8] Erasmus University Medical Center, Rotterdam, The Netherlands

32   [9] Department of Child and Adolescent Psychiatry/Psychology, Erasmus University Medical

33   Center - Sophia Children's Hospital, Rotterdam, The Netherlands

34   [10] Department of Neuroradiology & TUM-Neuroimaging Center (TUM-NIC), Klinikum

35   rechts der Isar, Technische Universität München, Munich, Germany

36   [11] Graduate School of Systemic Neurosciences GSN, Ludwig-Maximilians-Universität,

37   Biocenter, Munich, Germany

38   [12] Departament de Psicologia Clínica i Psicobiologia, Universitat de Barcelona, Barcelona,

39   Spain

40   [13] Institut de Neurociències, Universitat de Barcelona, Barcelona, Spain

41   [14] Institut de Recerca Pediàtrica Hospital Sant Joan de Déu. Esplugues de Llobregat,

42   Barcelona, Spain

43   [15] Wellcome EPSRC Centre for Interventional and Surgical Sciences (WEISS), University

44   College London, London, United Kingdom

45   [16] Center for Neurobehavioral Genetics, University of California Los Angeles, Los Angeles,

46   USA

47   [17] Department of Psychiatry, Icahn School of Medicine at Mount Sinai, New York, USA

48   [18] Department of Clinical Genetics, Amsterdam Neuroscience, VU University Medical

49   Center, Amsterdam, The Netherlands

50

51 **Corresponding author**

52 Martijn P. van den Heuvel

53 Department of Complex Trait Genetics, Center for Neurogenomics and Cognitive Research,

54 Amsterdam Neuroscience, VU University Amsterdam, De Boelelaan 1085, 1081 HV

55 Amsterdam, The Netherland

56 Department of Clinical Genetics, Amsterdam Neuroscience, VU University Medical Center,

57 De Boelelaan 1117, 1081 HV Amsterdam, The Netherlands

58 E-mail address: m.p.vanden.heuvel@vu.nl

59

60 **Abstract**

61 Macroscale white matter pathways form the infrastructure for large-scale communication in

62 the human brain, a prerequisite for healthy brain function. Conversely, disruptions in the

63 brain's connectivity architecture are thought to play an important role in a wide range of

64 psychiatric and neurological brain disorders. Here we show that especially connections

65 important for global communication and network integration are involved in a wide range of

66 brain disorders. We report on a meta-analytic connectome study comprising in total 895

67 patients and 1,016 controls across twelve neurological and psychiatric disorders. We

68 extracted disorder connectome fingerprints for each of these twelve disorders, which were

69 then combined into a cross-disorder disconnectivity involvement map, representing the

70 involvement of each brain pathway across brain disorders. Our findings show connections

71 central to the brain's infrastructure are disproportionally involved across a wide range of

72 disorders. Connections critical for global network communication and integration display

73 high disturbance across disorders, suggesting a general cross-disorder involvement and

74 importance of these pathways in normal function. Taken together, our cross-disorder study

3

75   suggests a convergence of disconnectivity across disorders to a partially shared

76   disconnectivity substrate of central connections.

77

78   **Background**

79   The macroscale connectome is the anatomical substrate for effective communication and

80   integration of information between brain regions [1,2]. Highly connected brain regions have a

81   central role in this infrastructure forming a densely interconnected rich club core [4,5]. This

82   centralization of connectivity has been argued to provide several benefits for global neural

83   integration [6–8] and with that healthy brain function [9,10]. However, due to their central

84   embedding in the network, hub regions and associated connections have also been suggested

85   to be generally vulnerable to network disruption [11] and, as a result, disproportionally involved

86   in a wide range of brain disorders [12].

87

88   Disease-associated alterations in structural and functional brain connectivity have been

89   observed across a wide range of neurological and psychiatric disorders [13,14]. Potentially, these

90   disconnectivity patterns converge across disorders to the hypothesized vulnerable substrate of

91   central connections. Such convergence is further suggested by observations that multiple

92   neuropsychiatric disorders involve overlapping neural circuits [15,16], share genetic risk factors

93   [17–19], and display high comorbidity [20] and shared brain phenotypes [16]. However, so far,

94   disease connectome studies have mostly been focused on single or small sets of disorders,

95   and do not provide discriminative power to identify cross-disorder biological patterns of

96   white matter disconnectivity [21,22].

97

98   Combining diffusion MRI data from studies on psychiatric and neurological disorders

99   provides new opportunities to assess the vulnerability of central connections in the human

100   brain. Here, we performed a cross-disorder data analysis, integrating connectivity alterations

101   in a dataset comprising diffusion MRI data of in total 895 patients and 1,016 matched

102   controls across twelve different brain disorders. These include eight psychiatric disorders

103   (schizophrenia, bipolar disorder, attention deficit hyperactivity disorder, autism spectrum

104   disorder, major depressive disorder, obesity, obsessive-compulsive disorder, posttraumatic

105   stress disorder) and four neurological disorders (Alzheimer's disease and its prodromal stage

106   known as mild cognitive impairment, amyotrophic lateral sclerosis and primary lateral

107   sclerosis). By combining disconnectivity maps of these twelve brain disorders we constructed

108   a 'cross-disorder involvement map', identifying the set of white matter pathways that show

109   involvement in multiple brain disorders. We combine this cross-disorder map with results

110   from network analysis of the human connectome and show that connections important for

111   neural integration are disproportionally involved across a range of disease processes.

112

113   **Results**

114   *Cross-disorder involvement map*

115   We examined MRI data of 2,681 patients and controls across twelve brain disorders from

116   previously published studies and cohorts. Based on diffusion MRI data, white matter

117   pathways were reconstructed in all subjects and combined with individual T1 data into

118   connectome maps. Connectome maps were reconstructed according to a subdivision of the

119   Desikan-Killiany atlas (DK-219). Results obtained using a second, different, parcellation of

120   the Desikan-Killiany atlas (DK-114) are described below in the robustness analyses section.

121   Quality control and patient-control matching was performed per study (see Methods) after

122   which 895 patients and 1,016 matched controls were included for analysis. An overview of

123   the demographics is provided in Figure 1 and Table 1. For each disorder, connectivity

124   alterations were estimated in disconnectivity maps quantifying the differences in connectivity

125 strength (fractional anisotropy) between patients and controls. Disconnectivity maps were

126 constructed per dataset to ensure patients and controls were matched and aggregated into 12

127 disorders disconnectivity maps (Figure 2A). In each disorder, the top 15 % connections with

128 highest disconnectivity effects were selected as disorder "involved". A fixed number of

129 connections was selected in each disorder to ensure equal presence of all disorders in the final

130 cross-disorder involvement map.

131

132 Combining all individual disease maps, a group cross-disorder involvement map was then

133 formed by the percentage of disorders in which a connection was considered "disorder

134 involved" (Figure 2B). Network based statistics showed significantly large subnetworks of

135 connections with cross-disorder involvement above 35%, 40% and 45% (all $p < 0.05$, Figure

136 SI 1). The largest subnetwork contained of 34 regions and 82 connections, including

137 connections of the caudal anterior cingulate, caudal middle frontal, paracentral, posterior

138 cingulate, precentral, precuneus, superior frontal and superior parietal regions ($p = 0.0003$,

139 Figure 2E). Averaging cross-disorder involvement of adjacent connections to each region

140 provided a measure of region-wise cross-disorder involvement (Figure 2D). Regions with

141 significantly high cross-disorder involvement included sub-regions of the postcentral gyrus

142 ($\times 2.23$ more than in permuted cross-disorder involvement maps, $p = 0.0109$, FDR-corrected)

143 and precentral gyrus ($\times 2.19$ higher, $p = 0.0109$, FDR-corrected).

144

145 *Network measures*

146 *Rich club organization*

147 The vulnerability of the central rich club connections to disease effects was tested with

148 respect to a rich club core of hub regions identified as the top 15% highest degree regions in

149 the reference connectome map (degree > 14, Figure SI 2). Based on the identified rich club

150   core, 7.6% of the network connections were classified as *rich club connections*, describing

151   connections spanning between hub regions, 27.7% as *feeder connections*, describing

152   connections spanning between hub and peripheral regions and 64.7% as *local connections*,

153   describing connections between peripheral regions. Significant disproportional cross-disorder

154   involvement was seen among rich club connections as compared to local connections (24%

155   higher, $p = 0.0041$, Figure 3) and, to a lesser extent, as compared to feeder connections (17%

156   higher, $p = 0.0325$). No specific increase was observed among feeder compared to local

157   connections ($p = 0.1209$).

158

159   *Edge-wise centrality measures*

160   We investigated the vulnerability of central connections by examining the cross-disorder

161   involvement of 25% most central connections identified by edge-wise centrality measures.

162   The importance of connections for global network integration was measured by the edge-

163   betweenness centrality, counting the number of shortest topological paths through each

164   connection. Connections with high betweenness centrality were significantly more often

165   involved across disorders than in randomized cross-disorder involvement maps (27% higher,

166    $p = 0.0001$, Figure 4). An extended definition of global network integration is given by

167   network communicability which considers all possible walks between nodes in the network.

168   Connections with large edge-removal effect on the network communicability also showed

169   significantly higher cross-disorder involvement (12% higher, $p = 0.0304$), further suggesting

170   disproportionally high cross-disorder effects in connections central for global

171   communication. In contrast, connections with strong contribution to local network

172   organization, measured by the network clustering coefficient, did not show a predisposition

173   for cross-disorder involvement ($p = 0.7330$). Finally, cross-disorder involvement was 42%

7

174   increased among spatially long connections (>50 mm) in comparison with cross-disorder

175   involvement maps with permuted disconnectivity effects (p < 0.0001).

176

177   *Global FA effects*

178   To verify independence of the association between network measures and cross-disorder

179   involvement from global FA differences (as often reported in case-control studies [60,61]),

180   additional permutation testing was performed in which subject labels were permuted, with

181   now, per disease and dataset, the global FA distribution in patient and control groups

182   preserved. Connections with high betweenness centrality again showed significantly higher

183   cross-disorder involvement (24% increase, p < 0.0001). Connections with high edge-removal

184   effect on network communicability also showed significantly higher cross-disorder

185   involvement (13% increase, p = 0.0092). Cross-disorder involvement was also higher among

186   the spatially longest connections (>50 mm), with a 36% higher cross-disorder involvement as

187   compared to short connections (<50 mm, p < 0.0001).

188

189   *Robustness analyses*

190   High rich club involvement was also observed when classification of rich club, feeder and

191   local connections were based on a smaller (7% or 9% highest degree regions) or larger set of

192   hub regions (18% or 25% highest degree regions). For all sets of hub regions, the associated

193   rich club connections showed significantly higher cross-disorder involvement than the

194   associated local connections (24% - 26% higher, all p < 0.05, Figure SI 3). Also, rich club

195   connections showed significantly higher cross-disorder involvement compared to feeder

196   connections (14% - 22% higher, all p < 0.05, Figure SI 3) when connection classes were

197   based on a smaller (9%) or larger set of hub regions (18% or 25%).

198

199   The results obtained using central connections selected as the top 25% connections with

200   highest edge-wise centrality scores showed exemplarily for a range of percentages (5% -

201   45%) of central connections (Figure SI 4). Both smaller (10% and 15%) and larger sets (30%

202   - 45%) of connections with high edge betweenness showed significantly higher cross-

203   disorder involvement than seen in randomized cross-disorder involvement maps (18% - 32%

204   higher, all $p < 0.05$). For central connections identified by edge-removal effect on

205   communicability, larger sets of central connections (30% - 45%) showed significantly higher

206   cross-disorder involvement than in randomized cross-disorder involvement maps (11% - 12%

207   higher, all $p < 0.05$). Connections selected by their spatial wiring length showed at all

208   percentages (5% - 45%) significantly higher than expected cross-disorder involvement (25%

209   - 61% higher, all $p < 0.05$).

210

211   In each disorder, a fixed number of connections (15% of the connections in the reference

212   connectome map) was selected as disorder involved to ensure equal contribution of all

213   disorders to the cross-disorder involvement map. Validating the results obtained by selecting

214   15% of the connections as disorder involved, showed similar results at other reasonable

215   percentages of disorder involved connections (5%, 10%, 20% and 25%, Figure SI 5). Rich

216   club connections showed significantly higher cross-disorder involvement compared with

217   local connections at all percentages (13% - 37% higher, all $p < 0.05$). Compared with feeder

218   connections, rich club connections showed significantly higher cross-disorder involvement at

219   the strict 5% (32% higher, $p = 0.0241$) and 10% (24% higher, $p = 0.0135$) percentages.

220   Moreover, significantly increased cross-disorder involvement was observed among central

221   connections selected by edge betweenness (18% - 42% higher, all $p < 0.05$) and spatial

222   wiring length (30% - 63% higher, all $p < 0.05$) at all percentages. Central connections

223   selected by edge-removal effect on communicability showed significantly higher cross-

9

224   disorder involvement, when selecting the stricter set of 10% of the connections as disorder

225   involved (15% higher, p = 0.0288).

226

227   To verify that the results were not driven by a single disorder, we performed a leave-one-out

228   analysis in which all analyses were repeated leaving out one disorder at a time

229   (Supplementary Materials). Results of the leave-one-out analysis showed in all iterations

230   significantly higher cross-disorder involvement of rich club connections relative to local

231   connections but not relative to feeder connections. The association between central

232   connections selected by edge betweenness, edge-removal effect on communicability and

233   spatial wiring length remained significant in all iterations (all p < 0.05, see Supplementary

234   Materials).

235

236   Using a second parcellation atlas, we further investigated cross-disorder involvement of

237   connections (Supplementary Materials). First, repeating the analysis revealed a subnetwork

238   of connections with increased cross-disorder involvement similar to the network reported in

239   the main analysis (p = 0.0002). Second, testing the vulnerability of central connections

240   confirmed the strong findings of the main text including: significantly higher cross-disorder

241   involvement of rich club connections compared to local connections (p = 0.0207) and

242   strongly elevated cross-disorder involvement was observed among connections with high

243   betweenness scores (p = 0. 0018) and spatial wiring length (p = 0.0001).

244

245   **Discussion**

246   Our findings show that connections central to network integration and communication in the

247   human brain are hotspots for white matter disconnectivity. Cross-disorder disconnectivity

248   was examined in 895 patients and 1,016 matched controls across a range of twelve

249 psychiatric and neurological disorders. Our findings provide three lines of evidence that

250 support a general vulnerability of central connections.

251

252 First, rich club connections showed significantly higher cross-disorder involvement as

253 compared to connections of peripheral regions (Figure 3). This observation is in line with

254 studies showing the involvement of hub regions in specific disorders, such as schizophrenia

255 [62], autism spectrum disorder [63], ADHD [63], Huntington's disease [64], Alzheimer's disease [65–67],

256 and general white matter lesions [68]. High involvement of rich club connections across

257 disorders is further in line with studies on cross-disorder gray matter abnormalities. A large

258 voxel-based morphometry meta-analysis showed hub regions to be disproportionally

259 involved in anatomical abnormalities across clinical brain disorders [12], findings verified by

260 voxel-based morphometry meta-analysis across clinical psychiatric disorders, showing shared

261 gray matter loss in in particular dorsal anterior cingulate and insula hub regions [15].

262

263 Second, edgewise network measures revealed connections critical for network efficiency and

264 communicability to display high cross-disorder involvement (Figure 4). This result extends

265 earlier reported decreased efficiency of structural networks in for example depression [65] and

266 in Alzheimer's disease, schizophrenia, multiple sclerosis and ALS (see [22] for a review),

267 suggesting that these effects are not disease-specific, but perhaps more general to brain

268 disorders than previously reported. Furthermore, these results stress the hypothesized

269 importance of efficient integration of information for healthy brain function [3], with

270 disruptions in central connections potentially leading to disproportional effects in brain

271 dysfunction.

272

273   A third line of evidence for the vulnerability of central connections is the observation of high

274   cross-disorder involvement among connections spanning long physical distances (Figure 4).

275   This observation is in line with studies reporting affected long fiber tracts including the

276   superior and inferior longitudinal fasciculus in for example ADHD [69], ASD [70], OCD [71], and

277   schizophrenia [72,73]. Post-hoc analysis showed these effects to be reduced when restricting the

278   analysis to intrahemispheric connectivity of either the left (19% increase, $p = 0.0190$) and

279   right hemisphere ($p = 0.0743$ (n.s.)), suggesting high cross-disorder involvement of spatially

280   long connections to be partly driven by a clustering of effects among interhemispheric

281   connections.

282

283   The observed cross-disorder effects are likely to reflect the combination of multiple disease

284   mechanisms that differ across disorders [74,75]. Central regions and connections have been

285   argued to be biologically expensive, characterized by complex neuronal architecture [76], high

286   metabolism [3] and high neuronal activity [77]. This high biological cost might result in increased

287   vulnerability to a wide range of disease processes, such as a toxic environment or reductions

288   in the supply of oxygen or other metabolic resources [78]. Central connections may also display

289   a high cross-disorder involvement as the result of their topological centrality and associated

290   risk to propagating disease processes [75,79]. Connectome studies of disconnectivity in ALS [80],

291   Alzheimer's disease [79,81,82] and frontal temporal dementia [82] have suggested a prion-type of

292   spread of disease processes in neurodegenerative disorders with specifically early disease

293   involvement of hub regions and rich club connections due to their central embedding in the

294   network. In addition to this, long-range central connections may be particularly vulnerable to

295   focal white matter degeneration. The chance of focal degeneration is proportional to fiber

296   length, making long-range central connections in total more vulnerable to general white

297   matter atrophy as compared to short range connections. Rich club connections have also been

298 shown to display a prolonged development [83–85], which may further increase their general

299 vulnerability by putting these connections at risk to late neurodevelopmental stress, substance

300 use and dysregulation of hypothalamic-pituitary-adrenal axis function [74,86]. The shared

301 vulnerability of central connections across disorders might result from the importance of

302 central connections for cognitive function [4,87]. Cognitive impairment is shared across the

303 symptomatology of many brain disorders [88]. Hence, if in each disorder separately

304 disconnectivity of central connections is associated with deficits in cognitive function, then

305 such overlap in symptomatology would result in general vulnerability of central connections.

306

307 Genetics and heritability studies offer the potential to gain further understanding in the

308 pathology underlying cross-disorder disconnectivity. Shared genetic etiology is observed

309 across many psychiatric and neurological disorders [17,89,90], with shared genetic risk factors

310 providing converging evidence for common underlying biological processes across brain

311 disorders [16,17,91]. Further exploring structural disconnectivity and genetic information in a

312 multi-modal and cross-disorder approach may further identify cross-disorder as well as

313 disorder-specific biological pathways [16,92–94].

314

315 The observation of overlapping disconnectivity patterns across brain disorders is in

316 agreement with the hypothesis that brain disorders are interrelated [17] and prompts for a

317 careful consideration of disease disconnectivity findings. Disconnectivity findings of single-

318 disorder connectome examinations may often be interpreted as disorder-specific

319 disconnectivity effects, which might not fully be the case considering the demonstrated

320 overlap in effects across disorders. This misattribution is perhaps most problematic in the

321 development of biomarkers for brain disorders based on disconnectivity fingerprints, where it

322 could result in overestimation of the disorder specificity of a presented biomarker.

13

323

324   Methodological issues have to be considered when interpreting our findings. While

325   combining data from multiple studies may implicitly account for real-world heterogeneity

326   and improve generalizability of observed results [95], it is likely that combining data from

327   multiple studies may also reduce statistical power as a result of inter-study heterogeneity in

328   diagnoses, demographics, scanner and MRI acquisition protocols. We are aware of this

329   limitation and aimed to minimize the influence of study specific properties by directly

330   comparing control and patient data within each study first, before combining information

331   across the twelve disorders. Second, disorder disconnectivity fingerprints were based on

332   structural brain networks obtained by diffusion-based MRI, with white matter microstructural

333   integrity assessed by means of the metric of fractional anisotropy [47]. Fractional anisotropy is

334   however only an indirect marker of the micro-scale neuroarchitecture and diffusion weighted

335   imaging has recognized limitations with respect to the reconstruction of complex fibers and

336   connectome mapping [45,96,97], which might result in underestimation of disconnectivity effects

337   within and across disorders. Third, our conclusions are based on effects seen across twelve

338   disorders, and it remains unclear whether our conclusions could be generalized to an even

339   wider range of brain disorders. To verify that the results were not driven by a single disorder,

340   we performed a leave-one-out validation analysis in which all analyses were repeated leaving

341   out one disorder at a time. Moreover, we possibly missed smaller sets of disorders that share

342   disconnectivity patterns. Investigating potential clustering of disorders based on their

343   disconnectivity patterns would be of great interest to further provide new insights in more

344   detailed biological relationships between disorders.

345

346   Our findings suggest shared connectome pathology across neurological and psychiatric

347   disorders, with in particular high general vulnerability of connections central to neural

348   communication and integration. Beyond identifying cross-disorder disconnectivity, cross-

349   disorder examination has the important potential to show distinct disconnectivity patterns

350   between disorders. Future examination into both disorder-shared and disorder-specific

351   disconnectivity effects provides better understanding of which brain alterations are general

352   and which effects are unique for brain disorders, providing new ways for the development of

353   MRI based biomarkers for psychiatric and neurological disorders.

354

355   **Methods**

356   *Studies and subjects*

357   Diffusion MRI data of 2,681 patients and controls of twelve disorders were included. Data

358   included diffusion-weighted imaging (DWI) data of previously reported studies on

359   schizophrenia (two datasets available, set I and II) [23,24], bipolar disorder [25], attention deficit

360   hyperactivity disorder (ADHD) [26], autism spectrum disorder (ASD) [26], major depressive

361   disorder (MDD) [27], obesity, obsessive-compulsive disorder (OCD) [28], posttraumatic stress

362   disorder (PTSD, two datasets, set I and set II) (ADNI-DOD adni.loni.usc.edu and [29]), and

363   four neurological disorders, Alzheimer's disease (AD, two datasets, set I and set II) (ADNI

364   and [30,31]), mild cognitive impairment (MCI, two datasets, set I and set II) (ADNI and [30,31]),

365   amyotrophic lateral sclerosis (ALS) [32–34] and primary lateral sclerosis (PLS) [32–34]. Figure 1

366   provides an overview of all data included and a summary is provided in Table 1. Further

367   details including a description of MRI acquisition protocols and demographics are outlined in

368   the Supplementary Materials. Within each dataset, patients and controls were matched on

369   age, sex, scanner settings and where possible other demographics (procedure described in the

370   Supplementary Materials).

371

372   *Data processing*

15

373   *DWI Tractography.* Data preprocessing of DWI and T1-weighted images of individuals

374   included the following steps: the anatomical T1-weighted image was parcellated into 219

375   distinct cortical regions (111 left-hemispheric and 108 right-hemispheric regions) according

376   to a subdivision of FreeSurfer's Desikan-Killiany atlas [35,36] using FreeSurfer [37]. Using a

377   second different parcellation of the Desikan-Killiany atlas (DK-114) showed similar results

378   presented in the robustness analyses section and Supplemental Materials. Second, the

379   individual parcellation map was co-registered to the DWI data using an affine transformation

380   mapping of the T1-weighted image to the DWI image. Third, diffusion-weighted images

381   were corrected for eddy current distortions and head motion using the FMRIB Software

382   Library [38]. If reversed phase encoding data was available (datasets listed in SI Table 1),

383   susceptibility induced distortions were estimated and incorporated in the preprocessing [39].

384   Fourth, a tensor was fitted to the diffusion signals in each voxel using a robust tensor fitting

385   algorithm [40] and subsequently fractional anisotropy (FA) was derived [41]. Given the mostly

386   clinical diffusion MRI protocols used for data acquisition, simple deterministic tensor

387   reconstruction (DTI) (as compared to more advanced diffusion profile reconstruction

388   methods) was used to minimize the potential influence of false positives on network

389   reconstruction and subsequent computation of network metrics [42–44]. This relatively simple

390   reconstruction of the diffusion signal is a limitation of our cross-disorder examination,

391   potentially leading to incomplete reconstruction of complex fiber pathways and an

392   underestimation of cross-disorder disease effects [45]. Fifth, white matter pathways were

393   reconstructed using fiber assignment by continuous tracking (FACT) [46], with streamline

394   reconstruction starting from eight seeds in every cerebral white matter voxel. Fiber tracking

395   was continued until a streamline showed high curvature (> 45º), exited the brain mask, or

396   when a streamline entered a voxel with low fractional anisotropy (< 0.1). The mean FA value

16

397   of a streamline was computed as the weighted average FA value over all voxels that a

398   streamline passed.

399

400   *Network reconstruction.* For each individual dataset, reconstructed streamlines and cortical

401   parcellation were combined into a weighted network. The 219 cortical areas were chosen as

402   nodes in the network and two regions were considered connected if at least one reconstructed

403   streamline was found to touch both cortical regions. The weight of connections was taken as

404   the mean fractional anisotropy (FA) of streamlines involved [47].

405

406   **Cross-disorder analysis**

407   Cross-disorder examination of disorder-related disconnectivity was performed in two steps.

408   Patient and control data were *first* compared *within* each dataset (in contrast to the alternative

409   of pooling all data into one large dataset) to ensure that patients and controls were matched

410   on age, sex and other demographics and scanner settings. This comparison provided for each

411   disorder a disconnectivity map quantifying the differences in connectivity strength between

412   patients and matched controls. *Second*, disorder disconnectivity maps were combined *across*

413   the twelve disorders to determine the distribution of disconnectivity effects across network

414   connections of the brain. This two-step approach optimized comparability of data across

415   studies with different MRI acquisition protocols. In what follows, we describe this procedure

416   in more detail, including the construction of the disorder disconnectivity maps and the cross-

417   disorder involvement map, followed by the performed statistical analyses.

418

419   *Step 1: Disorder disconnectivity map*

420   Per disorder, a disconnectivity map was constructed by assessing the between-group

421   difference in FA of connections between patients and controls quantified by a Student's t-test

17

422   statistic. As such, we tested for lowered FA connectivity strength in the patient group

423   compared to the controls. Between-group analysis was performed for connections that were

424   present in 30% or more of the population of controls and patients to ensure sufficient

425   statistical power [33]. To correct for possible differences in degrees of freedom across

426   connections, t-test statistics were transformed to z-scores.

427   For the disorders PTSD, schizophrenia, Alzheimer's disease and MCI, for which

428   multiple datasets were available, a disorder disconnectivity map was first calculated *per*

429   *dataset* and then combined into an average disorder disconnectivity map using Stouffer's

430   method for combining independent tests by averaging the z-scores in the disorder

431   disconnectivity maps across datasets [48,49].

432   In total, this resulted in a disorder disconnectivity map for each of the 12 included

433   brain disorders. Next, the top 15% connections with highest z-scores were selected as the set

434   of most involved connections in that disorder, performing, per disorder, a proportional

435   thresholding on the disorder-specific disconnectivity map with a density of 15% [50]. Results

436   using 5%, 10%, 20% or 25% involved connections are presented in the robustness analyses

437   section.

438

439   *Step 2: Cross-disorder involvement map*

440   The twelve thresholded disorder disconnectivity maps were combined into a total *cross-*

441   *disorder involvement map*. To maximize comparability across studies and to avoid any

442   potential bias to one of the included datasets, connection effects were included for those

443   connections present in a reference group connectome map based on high-quality data of the

444   Human Connectome Project (HCP, 500 Subjects Release of the Human Connectome Project)

445   [51,52] (see Supplementary Materials for details on the HCP group connectome reconstruction).

446   Finally, a *cross-disorder involvement map* was formed by adding up all thresholded disorder

447 disconnectivity maps and dividing it by the number of disorders in which each connection

448 was present, thus computing per connection the percentage of disorders in which this

449 connection was involved.

450

451 *Network analysis*

452 The centrality of connections in the network structure was considered with respect to rich

453 club organization, edgewise global and local network measures and physical wiring length.

454 Metrics were computed on the HCP group connectome to ensure independence of the

455 examined datasets.

456   *Rich club organization.* Central connections were identified with respect to the rich

457 club organization describing the collective of high-degree hub regions [4]. Regional degree was

458 computed on the basis of the HCP group connectome with hub regions selected as regions

459 with a degree above 14 (top 13% regions with the highest regional degree, 29 regions, Figure

460 3, listed in SI Table 2). This set of regions was verified to display a rich club organization,

461 showing a higher-than-expected level of interconnectivity ($p < 0.0001$, compared with 10,000

462 degree-preserved rewired networks using permutation testing).

463   Based on the identified rich club organization, network connections were classified

464 into *rich club connections*, describing connections spanning between hub regions, *feeder*

465 *connections*, describing connections spanning between hub and peripheral regions, or *local*

466 *connections*, describing connections between peripheral regions [6]. Analyses were repeated

467 with connections classes derived from a smaller and larger set of hub regions (top 7% highest

468 degree regions, degree > 16; top 9% highest degree regions, degree > 15; top 18% highest

469 degree regions, degree > 13 and top 25% highest degree regions, degree > 12).

470   *Global network organization.* Global network integration was examined from the

471 perspective of the ease of communication between nodes in the network. First, the centrality

472   of connections with respect to the shortest topological paths in the network was measured by

473   counting the number of shortest topological paths through each network connection using the

474   metric of edge betweenness [53]. Second, network integration was considered by examining the

475   metric of network communicability, measuring all possible walks between nodes [54]. The

476   contribution of connections to communicability was assessed by edge-removal statistics [55–57].

477   Removal-effect of each connection on network communicability was quantified as the

478   difference (in terms of percentage) between the network communicability before and after

479   removal of a connection.

480   *Local network organization.* The role of network connections in local network

481   organization was assessed through the contribution of each connection to *network clustering*

482   [53]. The removal-effect of each connection on global network clustering was quantified as the

483   difference (i.e., percentage of change) in global clustering before and after removal of the

484   connection.

485   *Spatial embedding.* Projection length of each connection was calculated as the

486   average physical length of a connection.

487

488   *Statistical analysis*

489   *Cross-disorder involvement.* Significant subnetworks in the brain with increased cross-

490   disorder involvement levels were identified using Network Based Statistics [59]. The cross-

491   disorder involvement map was binarized by including connections with cross-disorder

492   involvement percentages above a specified NBS-threshold. Multiple NBS-thresholds (0%,

493   5%, …, 100%) were considered, capturing the trade-off between specificity and sensitivity of

494   the NBS-analysis. The number of connections in the greatest component of the thresholded

495   network was counted. Significance of this cluster was assessed using permutation testing by

496   comparison with the distribution of greatest component sizes in a null condition in which

497 disease effects were randomized. For this, for each permutation, a cross-disorder involvement

498 map was calculated on a permuted subject sample in which subject labels (i.e. controls and

499 patients) were randomly reassigned (keeping patient and control group sizes intact). 10,000

500 permutations were examined and the percentage of the permutations in which the greatest

501 component was larger or equal to the observed greatest component was assigned as p-value

502 to the observed cross-disorder involvement. Regions with significantly high cross-disorder

503 involvement were similarly identified by comparison with the sample of subject-label

504 permuted cross-disorder involvement maps. To correct for multiple testing, p-values were

505 adjusted by the false discovery rate correction procedure [58].

506

507 *Network measures.* Differences in mean cross-disorder involvement between rich club

508 and feeder, rich club and local, and feeder and local connection classes were statistically

509 assessed using permutation testing (10,000 permutations). In each permutation, connection

510 class labels were randomly shuffled and mean cross-disorder involvement of the classes was

511 computed over the permuted connections. Differences in cross-disorder involvement between

512 connection classes were computed for all permutations. The observed difference in cross-

513 disorder involvement between two connection classes was assigned a p-value by computing

514 the percentage of permutations in which the difference between the two connection classes

515 was equal to or exceeded the observed difference.

516 The 25% connections most central connections selected by global network

517 integration, local network integration and the spatial embedding were examined. Exploring

518 other reasonable percentages (5%, 10%, …, 45%) for selecting central connections showed

519 consistent results that are reported in the robustness analyses. Cross-disorder involvement

520 levels were compared with the levels expected when disconnectivity was randomly

521 distributed using permutation testing, this to verify independence of our results from

21

522   connection properties such as connection prevalence or group-average connection strength.

523   For each permutation, subject labels were randomly reassigned and cross-disorder

524   involvement maps were calculated using the permuted subject-labeling. 10,000 permutations

525   were computed and cross-disorder involvement levels of the subsets of central connections

526   were calculated for each permutation. Based on this null distribution, the original effect was

527   assigned a p-value as the percentage of permutations in which the cross-disorder involvement

528   was equal to or exceeded the observed cross-disorder involvement.

529

530   *Global FA effects*

531   Additional permutation testing was performed to verify independence of our results from

532   global FA differences that are often reported in case-control studies[60,61]. For each subject,

533   global FA was computed as the total FA strength of all connections. Next, subjects were

534   classified into ten global FA groups, group one with global FA in the interval [0, 0.1), group

535   two with global FA in the interval [0.1, 0.2), etc. For permutation testing, subject labels were

536   permuted within datasets, but now under the constraint of only allowing switching patient

537   and control labels of subjects assigned to the same global FA bin. As such, the resulting

538   global FA distribution of permuted patient and control groups was kept similar to the original

539   global FA distributions (and therewith also potential between-group differences in global

540   FA). 10,000 permutations were computed and, in each permutation, the cross-disorder

541   involvement of the subsets of connections was calculated. Observed effects were assigned a

542   p-value as the percentage of the permutations in which the measured effect was equal to or

543   exceeded the observed effect.

544

545

546   **Acknowledgements**

572 grantee organization is the Northern California Institute for Research and Education, and the

573 study is coordinated by the Alzheimer's Therapeutic Research Institute at the University of

574 Southern California. ADNI data are disseminated by the Laboratory for Neuro Imaging at the

575 University of Southern California.

576

577 **Figures**

578 **Figure 1. Demographics.** Age distribution of controls (top) and patients (bottom) for all

579 twelve examined disorders. Age ranged between 6 – 90 years. Controls and patients within

580 datasets were matched on age and gender.

581

582 **Figure 2. Cross-disorder involvement. (A)** Overview of data aggregation and analysis. Per

583 disorder, a connection-wise disorder-specific disconnectivity map was computed contrasting

584 the fractional anisotropy of connections in patients and matched controls. Disorder-specific

585 disconnectivity maps were combined to determine the disconnectivity distribution across

586 disorders. **(B)** Schematic representation of human reference connectome with connections

587 colored by cross-disorder involvement. **(C)** Superior (left panel) frontal (right-top panel) and

588 medial (right-bottom panel) view of brain connectivity colored by cross-disorder

589 involvement. **(D)** Lateral and medial view of left and right hemispheres showing region-wise

590 cross-disorder involvement. **(E)** Network including 34 regions (colored blue) that showed

591 significant involvement across disorders (NBS analysis, p = 0.0003).

592

593 **Figure 3. Rich club organization. (A)** Cross-disorder involvement of rich club connections

594 was significantly 24% higher as compared to the set of local connections (p = 0.0041) and

595 17% higher than observed in the set of feeder connections (p = 0.0325). Error bars mark the

596 standard deviation. **(B)** Hub regions (top 13% highest degree regions, 29 regions) are colored

24

597   in red. **(C)** Schematic representation of human reference connectome with rich club

598   connections (colored red), feeder connections (orange) and local connections (yellow).

599

600   **Figure 4. Edgewise network measures.** From left to right, average cross-disorder

601   involvement of connections with highest edge betweenness centrality (top 25% shown),

602   highest edge-removal effect on communicability, highest edge removal effect on clustering

603   and long-distance connections. Observed values (blue) were compared with average cross-

604   disorder involvement in subject-label permuted maps (grey). Connections important for

605   global topological (edge betweenness centrality, and communicability) and spatial (long-

606   distance connections) integration showed significantly higher cross-disorder involvement

607   levels than expected for randomly distributed disease effects (indicated by an asterisk *, $p <$

608   0.05).

609

610   **Figure SI 1. Subnetworks identified by network based statistics. (A)** Number of regions

611   in the greatest component in thresholded version of the cross-disorder involvement map

612   across a range of thresholds (0% - 100% cross-disorder involvement). The greatest

613   components ranged from including all regions (at 0% cross-disorder involvement threshold)

614   to including only one region (at 100% cross-disorder involvement threshold). At 35%, 40%

615   and 45% cross-disorder involvement thresholds, the identified subnetwork showed

616   significantly larger than subnetwork seen in subject-label permuted cross-disorder

617   involvement maps (indicated by an asterisk *, $p < 0.05$). **(B)** Subnetworks and included

618   regions (in blue) of the three identified significantly large subnetworks.

619

620   **Figure SI 2. Rich club coefficient in reference connectome.** Reference connectome data

621   showed a significant rich club organization at all degree levels above 8 (indicated by an

622   asterisk *, p < 0.05, FDR-corrected).

623

624   **Figure SI 3. Rich club organization across percentages of hub regions.** Ratio between

625   cross-disorder involvement of rich club and local connections (left) and feeder connections

626   (right). The ratios were evaluated for rich club, feeder and local connections derived from

627   sets of hub regions selected at different percentages (7%, degree > 16; 9%, degree > 15; 13%,

628   degree > 14; 18%, degree > 13; 25%, degree > 12). Percentages at which the ratio was

629   significantly large (i.e. significant differences in cross-disorder involvement of rich club

630   connections and feeder or local connections) are indicated by an asterisk * (p < 0.05).

631

632   **Figure SI 4. Edgewise network measures across percentages of central connections.** The

633   cross-disorder involvement of central connections (selected by edge betweenness (left), edge-

634   removal effect on communicability (middle) and spatial wiring length (right)) relative to

635   cross-disorder involvement observed in subject-label permuted cross-disorder involvement

636   maps. The relative cross-disorder involvement was obtained at different selection percentages

637   ranging from considering the top 5% most central connections to the top 45% most central

638   connections. Percentages at which the ratio was significantly high (i.e. the set of central

639   connections showed significantly higher cross-disorder involvement than in permuted cross-

640   disorder involvement maps) are indicated by an asterisk * (p < 0.05).

641

642   **Figure SI 5. Cross-disorder involvement of central connections across percentages of**

643   **disorder involved connections.** Results were computed across various percentages of

644   connections selected as disorder involved in addition to the 15% percentage used in the main

26

645   analysis. **(A)** The ratio in cross-disorder involvement between rich club and local (left) and

646   feeder (right) connections. **(B)** The relative cross-disorder involvement of central connections

647   compared with subject-label permuted cross-disorder involvement maps. Significant effects

648   are indicated by an asterisk * ($p < 0.05$).

649

650   **Table 1.** Demographics after data quality control and matching.

651

652   **SI Table 1.** Acquisition parameters of included datasets.

653

654   **SI Table 2.** Number of excluded subjects (because subjects miss information, subjects are

655   considered outlier, or subjects are not matched) per dataset.

656

657   **SI Table 3.** List of hub regions (region subnumbers are study specific).

658

659   **References**

660   1.   Sporns, O., Tononi, G. & Kötter, R. The human connectome: A structural description

661   of the human brain. *PLoS Comput. Biol.* **1,** e42 (2005).

662   2.   Bullmore, E. & Sporns, O. The economy of brain network organization. *Nat. Rev.*

663   *Neurosci.* **13,** 336 (2012).

664   3.   Bullmore, E. & Sporns, O. The economy of brain network organization. *Nat. Rev.*

665   *Neurosci.* **13,** 336–49 (2012).

666   4.   van den Heuvel, M. P. & Sporns, O. Rich-Club Organization of the Human

667   Connectome. *J. Neurosci.* **31,** 15775–15786 (2011).

668   5.   van den Heuvel, M. P., Bullmore, E. T. & Sporns, O. Comparative Connectomics.

669   *Trends Cogn. Sci.* (2016). doi:10.1016/j.tics.2016.03.001

670   6.   van den Heuvel, M. P., Kahn, R. S., Goñi, J. & Sporns, O. High-cost, high-capacity

671   backbone for global brain communication. *Proc. Natl. Acad. Sci. U. S. A.* **109,** 11372–

672   7 (2012).

673   7.   Vertes, P. E., Alexander-Bloch, A. & Bullmore, E. T. Generative models of rich clubs

674   in Hebbian neuronal networks and large-scale human brain networks. *Philos. Trans. R.*

675   *Soc. B Biol. Sci.* **369,** 20130531–20130531 (2014).

676   8.   Senden, M., Deco, G., de Reus, M. A., Goebel, R. & van den Heuvel, M. P. Rich club

677   organization supports a diverse set of functional network configurations. *Neuroimage*

678   **96C,** 174–182 (2014).

679   9.   Baggio, H. C. *et al.* Rich Club Organization and Cognitive Performance in Healthy

680   Older Participants. *J. Cogn. Neurosci.* **27,** 1801–1810 (2015).

681   10. Ball, G. *et al.* Rich-club organization of the newborn human brain. *Proc. Natl. Acad.*

682   *Sci. U. S. A.* **111,** 7456–61 (2014).

683   11. van den Heuvel, M. P. & Sporns, O. Network hubs in the human brain. *Trends Cogn.*

684   *Sci.* **17,** 683–696 (2013).

685   12. Crossley, N. A. *et al.* The hubs of the human connectome are generally implicated in

686   the anatomy of brain disorders. *Brain* **137,** 2382–2395 (2014).

687   13. Catani, M. & ffytche, D. H. The rises and falls of disconnection syndromes. *Brain* **128,**

688   (2005).

689   14. Braun, U. *et al.* in *eLS* 1–9 (John Wiley & Sons, Ltd, 2015).

690   doi:10.1002/9780470015902.a0025783

691   15. Goodkind, M. *et al.* Identification of a common neurobiological substrate for mental

692   illness. *JAMA psychiatry* **72,** 305–315 (2015).

693   16. Lee, P. H. *et al.* Partitioning heritability analysis reveals a shared genetic basis of brain

694   anatomy and schizophrenia. *Mol. Psychiatry* **21,** 1680–1689 (2016).

695   17.   Doherty, J. L. & Owen, M. J. Genomic insights into the overlap between psychiatric

696   disorders: implications for research and clinical practice. *Genome Med.* **6,** 29 (2014).

697   18.   Anttila, V. *et al.* Analysis of shared heritability in common disorders of the brain.

698   *bioRxiv* (2016). doi:http://dx.doi.org/10.1101/048991

699   19.   O'Dushlaine, C. *et al.* Psychiatric genome-wide association study analyses implicate

700   neuronal, immune and histone pathways. *Nat. Neurosci.* **18,** 199–209 (2015).

701   20.   Nuyen, J. *et al.* Comorbidity was associated with neurologic and psychiatric diseases:

702   A general practice-based controlled study. *J. Clin. Epidemiol.* **59,** 1274–1284 (2006).

703   21.   Fornito, A. & Bullmore, E. T. Connectomics: A new paradigm for understanding brain

704   disease. *Eur. Neuropsychopharmacol.* **25,** 733–748 (2015).

705   22.   Griffa, A., Baumann, P. S., Thiran, J.-P. & Hagmann, P. Structural connectomics in

706   brain diseases. *Neuroimage* **80,** 515–526 (2013).

707   23.   Svatkova, A. *et al.* Physical Exercise Keeps the Brain Connected: Biking Increases

708   White Matter Integrity in Patients With Schizophrenia and Healthy Controls.

709   *Schizophr. Bull.* **41,** 869–78 (2015).

710   24.   Collin, G., Kahn, R. S., de Reus, M. A., Cahn, W. & van den Heuvel, M. P. Impaired

711   Rich Club Connectivity in Unaffected Siblings of Schizophrenia Patients. *Schizophr.*

712   *Bull.* **40,** 438–448 (2014).

713   25.   Collin, G. *et al.* Brain network analysis reveals affected connectome structure in

714   bipolar I disorder. *Hum. Brain Mapp.* **37,** 122–134 (2016).

715   26.   van Belle, J., van Hulst, B. M. & Durston, S. Developmental differences in intra-

716   individual variability in children with ADHD and ASD. *J. Child Psychol. Psychiatry*

717   **56,** 1316–1326 (2015).

718   27.   Repple, J. *et al.* A voxel-based diffusion tensor imaging study in unipolar and bipolar

719   depression. *Bipolar Disord.* **19,** 23–31 (2017).

29

720 28. Reess, T. J. *et al.* Connectomics-based structural network alterations in obsessive-

721   compulsive disorder. *Transl. Psychiatry* **6,** e882 (2016).

722 29. Kennis, M. *et al.* Treatment Outcome-Related White Matter Differences in Veterans

723   with Posttraumatic Stress Disorder. *Neuropsychopharmacology* **40,** 2434–42 (2015).

724 30. Mancini, M. *et al.* Network attack simulations in Alzheimer's disease: The link

725   between network tolerance and neurodegeneration. in *2016 IEEE 13th International*

726   *Symposium on Biomedical Imaging (ISBI)* 237–240 (IEEE, 2016).

727   doi:10.1109/ISBI.2016.7493253

728 31. Serra, L. *et al.* Network-Based Substrate of Cognitive Reserve in Alzheimer's Disease.

729   *J. Alzheimer's Dis.* **55,** 421–430 (2016).

730 32. van der Burgh, H. K. *et al.* Deep learning predictions of survival based on MRI in

731   amyotrophic lateral sclerosis. *NeuroImage Clin.* (2016).

732   doi:10.1016/j.nicl.2016.10.008

733 33. Verstraete, E., Veldink, J. H., Mandl, R. C. W., van den Berg, L. H. & van den Heuvel,

734   M. P. Impaired Structural Motor Connectome in Amyotrophic Lateral Sclerosis. *PLoS*

735   *One* **6,** e24239+ (2011).

736 34. Walhout, R. *et al.* Brain morphologic changes in asymptomatic C9orf72 repeat

737   expansion carriers. *Neurology* **85,** 1780–8 (2015).

738 35. Cammoun, L. *et al.* Mapping the human connectome at multiple scales with diffusion

739   spectrum MRI. *J. Neurosci. Methods* **203,** 386–397 (2012).

740 36. Desikan, R. S. *et al.* An automated labeling system for subdividing the human cerebral

741   cortex on MRI scans into gyral based regions of interest. *Neuroimage* **31,** 968–80

742   (2006).

743 37. Fischl, B. *et al.* Automatically Parcellating the Human Cerebral Cortex. *Cereb. Cortex*

744   **14,** 11–22 (2004).

745   38.   Andersson, J. L. R. & Sotiropoulos, S. N. An integrated approach to correction for off-

746   resonance effects and subject movement in diffusion MR imaging. *Neuroimage* **125,**

747   1063–1078 (2016).

748   39.   Andersson, J. L. R., Skare, S. & Ashburner, J. How to correct susceptibility distortions

749   in spin-echo echo-planar images: Application to diffusion tensor imaging. *Neuroimage*

750   **20,** 870–888 (2003).

751   40.   Chang, L. C., Walker, L. & Pierpaoli, C. Informed RESTORE: A method for robust

752   estimation of diffusion tensor from low redundancy datasets in the presence of

753   physiological noise artifacts. *Magn. Reson. Med.* **68,** 1654–1663 (2012).

754   41.   Alexander, A. L., Lee, J. E., Lazar, M. & Field, A. S. Diffusion tensor imaging of the

755   brain. *Neurotherapeutics* **4,** 316–29 (2007).

756   42.   Zalesky, A. *et al.* Connectome sensitivity or specificity: which is more important?

757   *Neuroimage* **142,** 407–420 (2016).

758   43.   Thomas, C. *et al.* Anatomical accuracy of brain connections derived from diffusion

759   MRI tractography is inherently limited. *Proc. Natl. Acad. Sci. U. S. A.* **111,** 16574–9

760   (2014).

761   44.   de Reus, M. A. & van den Heuvel, M. P. Estimating false positives and negatives in

762   brain networks. *Neuroimage* **70,** 402–9 (2013).

763   45.   Maier-Hein, K. H. *et al.* The challenge of mapping the human connectome based on

764   diffusion tractography. *Nat. Commun.* **8,** 1349 (2017).

765   46.   Mori, S., Crain, B. J., Chacko, V. P. & van Zijl, P. C. M. Three-dimensional tracking

766   of axonal projections in the brain by magnetic resonance imaging. *Ann. Neurol.* **45,**

767   265–269 (1999).

768   47.   Beaulieu, C. The basis of anisotropic water diffusion in the nervous system - a

769   technical review. *NMR Biomed.* **15,** 435–455 (2002).

31

770   48.   Whitlock, M. C. Combining probability from independent tests: the weighted Z-

771   method is superior to Fisher's approach. *J. Evol. Biol.* **18,** 1368–1373 (2005).

772   49.   Riley, J. W. *et al.* The American Soldier: Adjustment During Army Life. *American*

773   *Sociological Review* **14,** 557 (1949).

774   50.   van den Heuvel, M. *et al.* Proportional thresholding in resting-state fMRI functional

775   connectivity networks and consequences for patient-control connectome studies:

776   Issues and recommendations. *Neuroimage* (2017).

777   doi:10.1016/j.neuroimage.2017.02.005

778   51.   Glasser, M. F. *et al.* The minimal preprocessing pipelines for the Human Connectome

779   Project. *Neuroimage* **80,** 105–24 (2013).

780   52.   Van Essen, D. C. *et al.* The Human Connectome Project: a data acquisition

781   perspective. *Neuroimage* **62,** 2222–31 (2012).

782   53.   Rubinov, M. & Sporns, O. Complex network measures of brain connectivity: uses and

783   interpretations. *Neuroimage* **52,** 1059–69 (2010).

784   54.   Estrada, E. & Hatano, N. Communicability in complex networks. *Phys. Rev. E* **77,**

785   36111 (2008).

786   55.   Irimia, A. & Van Horn, J. D. Systematic network lesioning reveals the core white

787   matter scaffold of the human brain. *Front. Hum. Neurosci.* **8,** 51 (2014).

788   56.   de Reus, M. A. & van den Heuvel, M. P. Simulated rich club lesioning in brain

789   networks: a scaffold for communication and integration? *Front. Hum. Neurosci.* **8,** 647

790   (2014).

791   57.   de Reus, M. A., Saenger, V. M., Kahn, R. S. & van den Heuvel, M. P. An edge-centric

792   perspective on the human connectome: link communities in the brain. *Philos. Trans. R.*

793   *Soc. London B Biol. Sci.* **369,** (2014).

794   58.   Benjamini, Y. & Hochberg, Y. Controlling the False Discovery Rate: A Practical and

795   Powerful Approach to Multiple Testing. *J. R. Stat. Soc. Ser. B …* **57,** 289–300 (1995).

796   59.   Zalesky, A., Fornito, A. & Bullmore, E. T. Network-based statistic: Identifying

797   differences in brain networks. *Neuroimage* **53,** 1197–1207 (2010).

798   60.   Sexton, C. E., Mackay, C. E. & Ebmeier, K. P. A Systematic Review of Diffusion

799   Tensor Imaging Studies in Affective Disorders. *Biol. Psychiatry* **66,** 814–823 (2009).

800   61.   Ellison-Wright, I. & Bullmore, E. Meta-analysis of diffusion tensor imaging studies in

801   schizophrenia. *Schizophr. Res.* **108,** 3–10 (2009).

802   62.   van den Heuvel, M. P. *et al.* Abnormal Rich Club Organization and Functional Brain

803   Dynamics in Schizophrenia. *JAMA Psychiatry* **70,** 783 (2013).

804   63.   Grayson, D. S. *et al.* Structural and functional rich club organization of the brain in

805   children and adults. *PLoS One* **9,** e88297 (2014).

806   64.   McColgan, P. *et al.* Selective vulnerability of Rich Club brain regions is an

807   organizational principle of structural connectivity loss in Huntington's disease. *Brain*

808   **138,** 3327–3344 (2015).

809   65.   Bai, F. *et al.* Topologically Convergent and Divergent Structural Connectivity Patterns

810   between Patients with Remitted Geriatric Depression and Amnestic Mild Cognitive

811   Impairment. *J. Neurosci.* **32,** (2012).

812   66.   Lo, C.-Y. *et al.* Diffusion tensor tractography reveals abnormal topological

813   organization in structural cortical networks in Alzheimer's disease. *J. Neurosci.* **30,**

814   16876–85 (2010).

815   67.   Yao, Z. *et al.* Abnormal Cortical Networks in Mild Cognitive Impairment and

816   Alzheimer's Disease. *PLoS Comput. Biol.* **6,** e1001006 (2010).

817   68.   Langen, C. D. *et al.* THE STRUCTURAL DISCONNECTOME : A PATHOLOGY-

818   SENSITIVE EXTENSION OF THE STRUCTURAL CONNECTOME Department of

819   Radiology and Nuclear Medicine , Erasmus MC , Rotterdam , The Netherlands

33

820   Department of Medical Informatics , Erasmus MC , Rotterdam , The Netherland. 366–

821   370 (2017).

822 69. Hamilton, L. S. *et al.* Reduced white matter integrity in attention-deficit hyperactivity

823   disorder. *Neuroreport* **19,** 1705–8 (2008).

824 70. Koldewyn, K. *et al.* Differences in the right inferior longitudinal fasciculus but no

825   general disruption of white matter tracts in children with autism spectrum disorder.

826   *Proc. Natl. Acad. Sci. U. S. A.* **111,** 1981–6 (2014).

827 71. Peng, Z. *et al.* Brain structural abnormalities in obsessive-compulsive disorder:

828   Converging evidence from white matter and grey matter. *Asian J. Psychiatr.* **5,** 290–

829   296 (2012).

830 72. Karlsgodt, K. H. *et al.* Diffusion Tensor Imaging of the Superior Longitudinal

831   Fasciculus and Working Memory in Recent-Onset Schizophrenia. *Biol. Psychiatry* **63,**

832   512–518 (2008).

833 73. Ashtari, M. *et al.* Disruption of White Matter Integrity in the Inferior Longitudinal

834   Fasciculus in Adolescents With Schizophrenia as Revealed by Fiber Tractography.

835   *Arch. Gen. Psychiatry* **64,** 1270 (2007).

836 74. Pantelis, C. *et al.* Structural Brain Imaging Evidence for Multiple Pathological

837   Processes at Different Stages of Brain Development in Schizophrenia. *Schizophr. Bull.*

838   **31,** 672–696 (2005).

839 75. Fornito, A., Zalesky, A. & Breakspear, M. The connectomics of brain disorders. *Nat.*

840   *Rev. Neurosci.* **16,** 159–172 (2015).

841 76. van den Heuvel, M. P., Scholtens, L. H., Feldman Barrett, L., Hilgetag, C. C. & de

842   Reus, M. A. Bridging Cytoarchitectonics and Connectomics in Human Cerebral

843   Cortex. *J. Neurosci.* **35,** 13943–13948 (2015).

844 77. de Haan, W., Mott, K., van Straaten, E. C. W., Scheltens, P. & Stam, C. J. Activity

845   Dependent Degeneration Explains Hub Vulnerability in Alzheimer's Disease. *PLoS*

846   *Comput. Biol.* **8,** e1002582 (2012).

847   78.   Buckner, R. L. *et al.* Cortical hubs revealed by intrinsic functional connectivity:

848   mapping, assessment of stability, and relation to Alzheimer's disease. *J Neurosci* **29,**

849   1860–1873 (2009).

850   79.   Iturria-Medina, Y. *et al.* Epidemic Spreading Model to Characterize Misfolded

851   Proteins Propagation in Aging and Associated Neurodegenerative Disorders. *PLoS*

852   *Comput. Biol.* **10,** e1003956 (2014).

853   80.   Schmidt, R., de Reus, M. A., Scholtens, L. H., van den Berg, L. H. & van den Heuvel,

854   M. P. Simulating disease propagation across white matter connectome reveals

855   anatomical substrate for neuropathology staging in amyotrophic lateral sclerosis.

856   *Neuroimage* **124,** 762–769 (2016).

857   81.   Zhou, J., Gennatas, E. D., Kramer, J. H., Miller, B. L. & Seeley, W. W. Predicting

858   Regional Neurodegeneration from the Healthy Brain Functional Connectome. *Neuron*

859   **73,** 1216–1227 (2012).

860   82.   Raj, A., Kuceyeski, A. & Weiner, M. A Network Diffusion Model of Disease

861   Progression in Dementia. *Neuron* **73,** 1204–1215 (2012).

862   83.   Wierenga, L. M. *et al.* A multisample study of longitudinal changes in brain network

863   architecture in 4-13-year-old children. *Hum. Brain Mapp.* **0,** (2017).

864   84.   Baker, S. T. E. *et al.* Developmental Changes in Brain Network Hub Connectivity in

865   Late Adolescence. *J. Neurosci.* **35,** 9078–87 (2015).

866   85.   Whitaker, K. J. *et al.* Adolescence is associated with genomically patterned

867   consolidation of the hubs of the human brain connectome. *Proc. Natl. Acad. Sci. U. S.*

868   *A.* **113,** 9105–10 (2016).

869   86.   Dennis, E. L. *et al.* Development of the 'rich club' in brain connectivity Networks

870   from 438 adolescents & adults aged 12 to 30. *Proceedings. IEEE Int. Symp. Biomed.*

871   *Imaging* 624–627 (2013). doi:10.1109/ISBI.2013.6556552

872 87. de Groot, J. C. *et al.* Cerebral white matter lesions and cognitive function: the

873   Rotterdam Scan Study. *Ann. Neurol.* **47,** 145–51 (2000).

874 88. Millan, M. J. *et al.* Cognitive dysfunction in psychiatric disorders: characteristics,

875   causes and the quest for improved therapy. *Nat. Rev. Drug Discov.* **11,** 141–168

876   (2012).

877 89. McLaughlin, R. L. *et al.* Genetic correlation between amyotrophic lateral sclerosis and

878   schizophrenia. *Nat. Commun.* **8,** 14774 (2017).

879 90. Cross-Disorder Group of the Psychiatric Genomics Consortium, C.-D. G. of the P. G.

880   *et al.* Genetic relationship between five psychiatric disorders estimated from genome-

881   wide SNPs. *Nat. Genet.* **45,** 984–94 (2013).

882 91. Schulze, T. G. *et al.* Molecular genetic overlap in bipolar disorder, schizophrenia, and

883   major depressive disorder. *World J. Biol. Psychiatry* **15,** 200–208 (2014).

884 92. Romme, I. A. C., de Reus, M. A., Ophoff, R. A., Kahn, R. S. & van den Heuvel, M. P.

885   Connectome Disconnectivity and Cortical Gene Expression in Patients With

886   Schizophrenia. *Biol. Psychiatry* (2016). doi:10.1016/j.biopsych.2016.07.012

887 93. Mufford, M. S. *et al.* Neuroimaging genomics in psychiatry—a translational approach.

888   *Genome Med.* **9,** 102 (2017).

889 94. Wang, T. *et al.* Polygenic risk for five psychiatric disorders and cross-disorder and

890   disorder-specific neural connectivity in two independent populations. *NeuroImage*

891   *Clin.* **14,** 441–449 (2017).

892 95. Sweeney, T. E., Haynes, W. A., Vallania, F., Ioannidis, J. P. & Khatri, P. Methods to

893   increase reproducibility in differential gene expression via meta-analysis. *Nucleic*

894   *Acids Res.* **45,** e1 (2017).

895   96.   van den Heuvel, M. P. *et al.* Comparison of diffusion tractography and tract-tracing

896   measures of connectivity strength in rhesus macaque connectome. *Hum. Brain Mapp.*

897   **36,** 3064–3075 (2015).

898   97.   Jbabdi, S. & Johansen-Berg, H. Tractography: where do we go from here? *Brain*

899   *Connect.* **1,** 169–83 (2011).

900

901

Figure 1. Demographics. Age distribution of controls (top) and patients (bottom) for all twelve examined disorders. Age ranged between 6 – 90 years. Controls and patients within datasets were matched on age and gender.
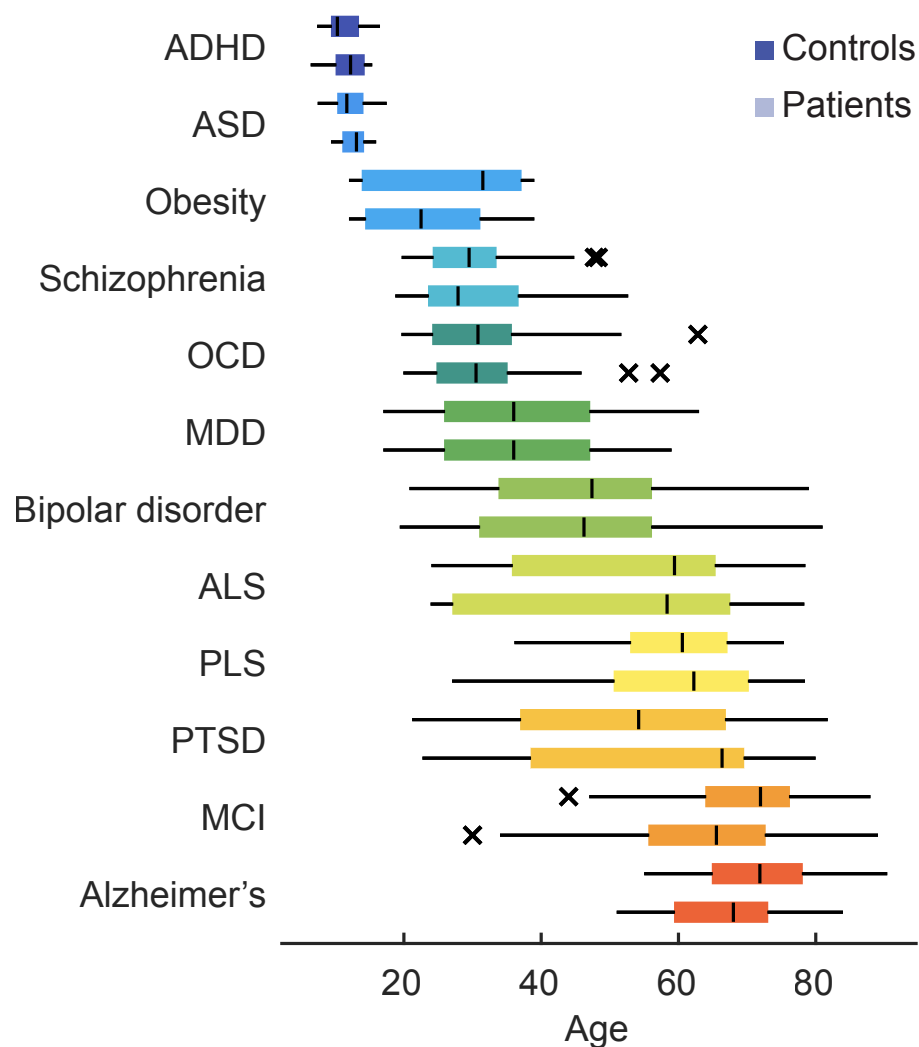
Figure 2. Cross-disorder involvement. (A) Overview of data aggregation and analysis. Per disorder, a connection-wise disorder-specific disconnectivity map was computed contrasting the fractional anisotropy of connections in patients and matched controls. Disorder-specific disconnectivity maps were combined to determine the disconnectivity distribution across disorders. (B) Schematic representation of human reference connectome with connections colored by cross-disorder involvement. (C) Superior (left panel) frontal (right-top panel) and medial (right-bottom panel) view of brain connectivity colored by cross-disorder involvement. (D) Lateral and medial view of left and right hemispheres showing region-wise cross-disorder involvement. (E) Network including 34 regions (colored blue) that showed significant involvement across disorders (NBS analysis, p = 0.0003).
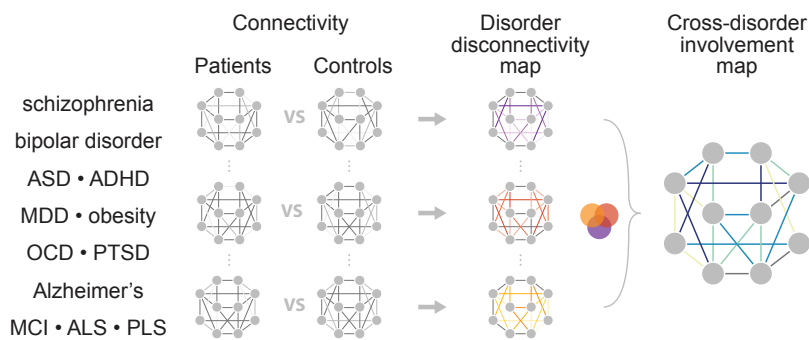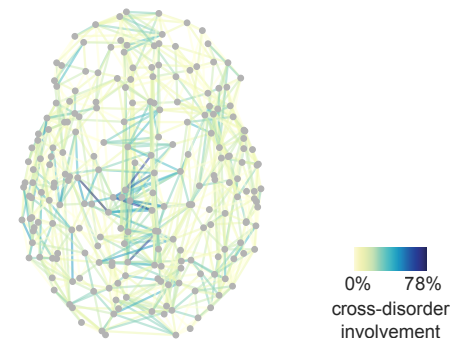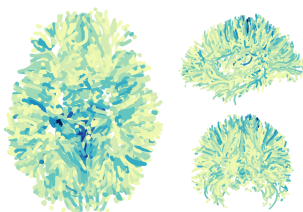
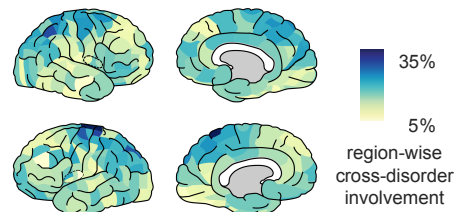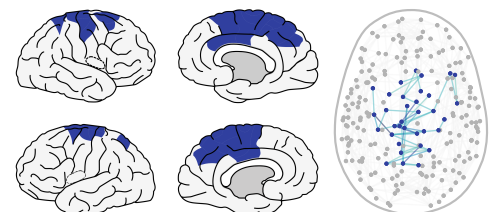**Figure 3. Rich club organization.** (A) Cross-disorder involvement of rich club connections was significantly 24% higher as compared to the set of local connections (p = 0.0048) and 17% higher than observed in the set of feeder connections (p = 0.0328). Error bars mark the standard deviation. (B) Hub regions (top 15% highest degree regions, 29 regions) are colored in red. (C) Schematic representation of human reference connectome with rich club connections (colored red), feeder connections (orange) and local connections (yellow).
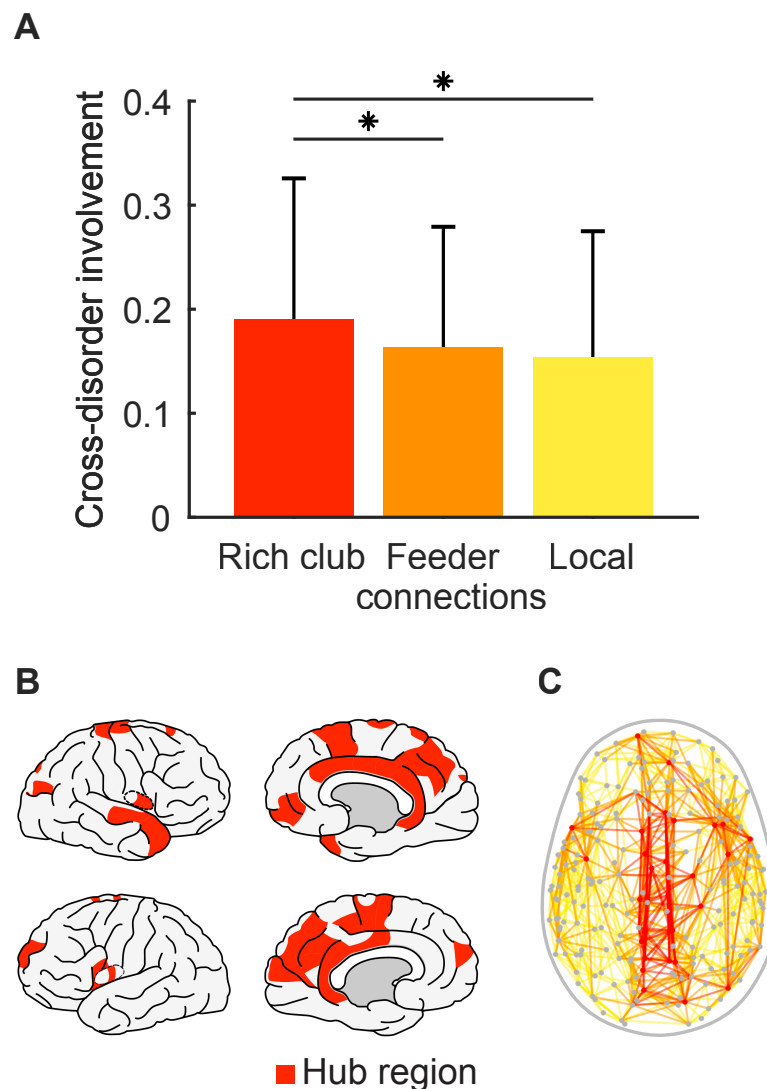
Figure 4. Edgewise network measures. From left to right, average cross-disorder involvement of connections with highest edge betweenness centrality (top 25% shown), highest edge-removal effect on communicability, highest edge removal effect on clustering and long-distance connections. Observed values (blue) were compared with average cross-disorder involvement in subject-label permuted maps (grey). Connections important for global topological (edge betweenness centrality, and communicability) and spatial (long-distance connections) integration showed significantly higher cross-disorder involvement levels than expected for randomly distributed disease effects (indicated by an asterisk *, $p < 0.05$).
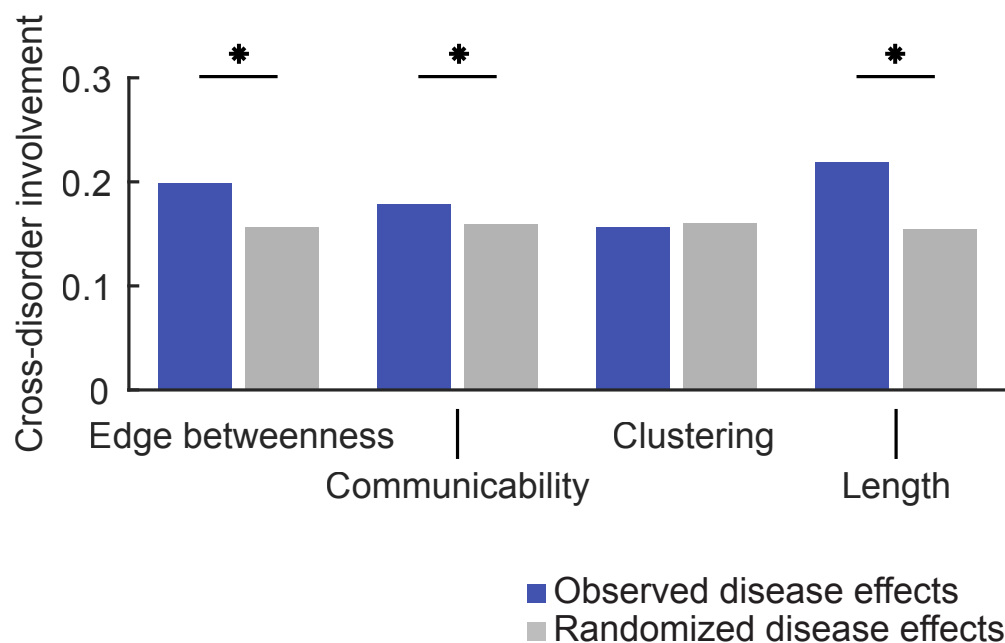
Table 1. Demographics after data quality control and matching.

| Disease | Nr. con. | Nr. pat. | Age | | | Sex | | | References |
			Con. mean (SD)	Pat. mean (SD)	P-value	Con. male/female (%/%)	Pat. male/female (%/%)	P-value	
ADHD	14	33	12.07 (2.48)	11.15 (2.54)	0.27	13/1 (92.9/.7.1)	27/6 (81.8/.18.2)	0.33	[1]
ALS	45	45	50.99 (19.10)	51.98 (15.98)	0.79	37/8 (82.2/.17.8)	33/12 (73.3/.26.7)	0.31	[2–4]
MCI I	28	28	57.89 (12.22)	62.79 (7.81)	0.09	15/13 (53.6/.46.4)	19/9 (67.9/.32.1)	0.27	[5]
MCI II	17	95	72.80 (6.74)	72.48 (7.22)	0.87	8/8 (50.0/.50.0)	56/33 (62.9/.37.1)	0.33	ADNI
OCD	41	36	31.71 (8.27)	31.50 (9.40)	0.92	18/23 (43.9/.56.1)	14/22 (38.9/.61.1)	0.66	[6]
PLS	32	32	59.18 (14.60)	59.93 (9.70)	0.81	19/13 (59.4/.40.6)	17/15 (53.1/.46.9)	0.61	[2–4]
PTSD I	25	45	36.92 (10.61)	37.98 (9.31)	0.67	25/0 (100.0/.0.0)	45/0 (100.0/.0.0)	1.00	[7]
PTSD II	40	40	69.86 (4.50)	68.04 (3.86)	0.06	40/0 (100.0/.0.0)	40/0 (100.0/.0.0)	1.00	DOD ADNI
Alzheimer's I	19	19	62.26 (7.45)	65.89 (5.75)	0.11	8/11 (42.1/.57.9)	11/8 (57.9/.42.1)	0.33	[5,8]
Alzheimer's II	16	37	72.24 (4.54)	75.04 (8.80)	0.24	5/8 (38.5/.61.5)	21/14 (60.0/.40.0)	0.18	ADNI
ASD	17	32	12.72 (1.84)	12.10 (2.48)	0.38	15/2 (88.2/.11.8)	27/5 (84.4/.15.6)	0.71	[1]
Bipolar disorder	82	82	45.18 (14.62)	45.86 (13.41)	0.76	42/40 (51.2/.48.8)	49/33 (59.8/.40.2)	0.27	[9]
MDD	478	211	37.19 (11.76)	36.93 (12.15)	0.79	210/268 (43.9/.56.1)	104/107 (49.3/.50.7)	0.19	[10]
Obesity	32	30	23.53 (8.66)	26.80 (10.72)	0.20	15/17 (46.9/.53.1)	10/20 (33.3/.66.7)	0.28	[11]
schizophrenia I	107	107	29.62 (7.54)	29.48 (7.38)	0.89	71/34 (67.6/.32.4)	83/24 (77.6/.22.4)	0.10	[12]
schizophrenia II	23	23	31.46 (7.36)	31.54 (3.23)	0.96	17/6 (73.9/.26.1)	18/5 (78.3/.21.7)	0.73	[13]